PNAS RESEARCH ARTICLE | NEUROSCIENCE OPEN ACCESS

Pten heterozygosity restores neuronal morphology in fragile X syndrome mice

Shivaprasad H. Sathyanarayana[a,1], Jasmine A. Saunders[a], Jacob Slaughter[a], Kamran Tariq[a], Rajarshi Chakrabarti[b], Madhumala K. Sadanandappa[a], Bryan W. Luikart[a,2], and Giovanni Bosco[a,2]

Edited by John Rubenstein, University of California, San Francisco, CA; received May 27, 2021; accepted February 11, 2022

Genetic studies of hippocampal granule neuron development have been used to elucidate cellular functions of *Pten* and *Fmr1*. While mutations in each gene cause neurodevelopmental disorders such as autism and fragile X syndrome, how *Pten* and *Fmr1* function alone or together during normal development is not known. Moreover, *Pten* mRNA is bound by the fragile X mental retardation protein (FMRP) RNA binding protein, but how this physical interaction impinges on phosphatase and tensin homolog protein (PTEN) expression is not known. To understand the interaction of PTEN and FMRP, we investigated the dentate gyrus granule neuron development in *Pten* and *Fmr1* knockout (KO) mice. Interestingly, heterozygosity of *Pten* restored *Fmr1* KO cellular phenotypes, including dendritic arborization, and spine density, while PTEN protein expression was significantly increased in *Fmr1* KO animals. However, complete deletion of both *Pten* and *Fmr1* resulted in a dramatic increase in dendritic length, spine density, and spine length. In addition, overexpression of PTEN in *Fmr1* KO *Pten* heterozygous background reduced dendritic length, arborization, spine density, and spine length including pS6 levels. Our findings suggest that PTEN levels are negatively regulated by FMRP, and some *Fmr1* KO phenotypes are caused by dysregulation of PTEN protein. These observations provide evidence for the genetic interaction of PTEN and FMRP and a possible mechanistic basis for the pathogenesis of *Fmr1*-related fragile X neurodevelopmental disorders.

Pten | Fmr1 | dentate gyrus | arborization | spine density

Significance

Phosphatase and tensin homolog protein (PTEN) and fragile X mental retardation protein (FMRP) play a vital role in neuronal development and function. This work provides new evidence for the genetic interaction of *Pten* and *Fmr1* in postnatal development of granule neurons and conserved mechanisms across evolution. The observed cellular phenotypic defects in *Pten* and *Fmr1* knockout (KO) could be rectified and restored by heterozygosity of *Pten* in *Fmr1* KO neurons. Additionally, increased expression of PTEN in background *Fmr1* KO animals suggests that FMRP negatively regulates PTEN, and we propose that introducing a combination of genetic mutations may normalize structural aspects of neuronal morphology by balancing each other's expression.

Neurons undergo remarkable structural complexification during development. Developmental disorders like fragile X syndrome (FXS) and some forms of autism spectrum disorder (ASD) are caused by mutations that alter the morphological development of neurons. *PTEN* is a tumor suppressor gene that encodes for phosphatase and tensin homolog protein (PTEN) and *FMR1* is a translational regulator that encodes for fragile X mental retardation protein (FMRP) (1–6). Loss of *Pten* in rodents causes macrocephaly, seizures, impaired social behaviors, and sensory hypersensitivity (7–11). short hairpin RNA-mediated knockdown of *Pten* led to an increase in the neuron soma size, dendrite arbor growth, dendritic shaft diameter, and dendritic spine density (12, 13). Cre-mediated *Pten* knockout (KO) demonstrates that neuronal hypertrophy is accompanied by an increase in inappropriate excitatory synapses and neuronal hyperactivity (5, 14).

FMRP is an RNA binding protein regulating the localization, stability, and translation of a large number of RNAs which are critical for neuronal development (15–17). Unstable CGG trinucleotide repeats (>200) in the 5′-untranslated regions of the *FMR1* gene causes hypermethylation and transcriptional silencing resulting in the loss of FMRP expression causing FXS (2, 18–20). In general, animal models and humans with FXS display an increased dendritic spine density with a greater number of filopodial protrusions compared to controls (21). While both PTEN and FMRP loss appear to result in an increased number of dendritic "spines," PTEN loss results in an increase in the number of stable spines and electrophysiologically defined synapses while FMRP loss results in an increase in unstable filopodial spines and a decrease in functional excitatory synapses.

Both *Pten* and *Fmr1* genes regulate the target of rapamycin (mTOR) signaling network (16, 22–25). FMRP regulates the expression of proteins in the mTORC1 pathway and disruption of mTORC1 signaling has been suggested to give rise to the FXS phenotype (2, 26). For example, overactivation of p70S6 kinase 1 (S6K1) in a FXS mouse model prompts mTORC1 signaling in hippocampal and cortical synapses (6, 27). By contrast, reduction of S6K1 activity in *Fmr1* KO mice rectifies the molecular signaling, restores spine morphology, and ASD-like behaviors (1, 28). *Tsc2* heterozygous mutations in the *Fmr1* KO background rescues the synaptic and behavioral

Author affiliations: [a]Department of Molecular and Systems Biology, Geisel School of Medicine at Dartmouth, Hanover, NH 03755; and [b]Department of Biochemistry and Cellular Biology, Geisel School of Medicine at Dartmouth, Hanover, NH 03755

Author contributions: S.H.S., B.W.L., and G.B. designed research; S.H.S., J.A.S., J.S., K.T., R.C., and B.W.L. performed research; S.H.S., J.A.S., J.S., K.T., R.C., M.K.S., and B.W.L. analyzed data; and S.H.S., M.K.S., B.W.L., and G.B. wrote the paper.

The authors declare no competing interest.

This article is a PNAS Direct Submission.

[1]Present address: Department of Pathology and Laboratory Medicine, Dartmouth Hitchcock Medical Center, Lebanon, NH 03766.

[2]To whom correspondence may be addressed. Email: Bryan.W.Luikart@dartmouth.edu or Giovanni.Bosco@dartmouth.edu.

This article contains supporting information online at http://www.pnas.org/lookup/suppl/doi:10.1073/pnas.2109448119/-/DCSupplemental.

Published April 8, 2022.

impairments of FXS (29). These observations suggest that cellular pathways in which PTEN and FMRP function may share multiple points of intersection, raising the possibility that ASD severity is modulated by interactions between genetic variants of some of these genes.

To understand the functional role of both PTEN and FMRP in neuronal development, and their genetic interactions, we investigated the dentate gyrus granule neuron development in *Pten* and *Fmr1* KO animals. In the *Fmr1* KO background, we introduced *Pten* heterozygous or homozygous loss, and examined neuron morphological development including dendritic arborization, spine density, and spine length. We show that heterozygous *Pten* loss could restore granule neuron cellular phenotypes in *Fmr1* KO mice. We found increased PTEN expression in the *Fmr1* KO mouse that is restored to normal levels by *Pten* heterozygosity. In addition, overexpression of PTEN in *Fmr1* KO *Pten* heterozygous background reduce dendritic arborization, length, spine density, spine length, and levels of pS6 in cells expressing excess PTEN. Thus, our genetic ablation study reveals FMR1 regulates PTEN expression and that partial genetic loss-of-function in *Pten* counteracts the up-regulation of PTEN protein in mouse models of FXS.

Results

Loss of FMRP Increases Total PTEN Protein Expression. Previous work has examined the specific RNA targets bound by the FMRP RNA binding protein (2, 30). We therefore hypothesized that the loss of FMRP affects the expression levels of PTEN protein. We used *Pten* and *Fmr1* germline KO mice derived from B6;129P2-*Pten*^{tm1Mak}/Mmjax (for PTEN) and B6.129P2-*Fmr1*$^{tm1Cgr/J}$ (for FMRP) to harvest the whole hippocampal tissue on P67. As expected, *Pten*^{Het} mice showed a significant reduction in PTEN protein levels (Fig. 1*A*; 50% decrease to wild type; $n = 6$ for wild type; $n = 5$ for *Pten*^{Het}; $P = 0.001$). Interestingly, *Pten*^{Het} hippocampal tissue was found to have increased FMRP expression compared to wild-type mice (40% increase to wild type; $n = 6$ wild type; $n = 5$ *Pten*^{Het}; $P = 0.001$, one-way ANOVA) (Fig. 1*B* and Dataset S1). Conversely, the hippocampi lysate of *Fmr1*^{KO} also showed a significant increase in the expression of PTEN protein levels (80% increase relative to wild type; $n = 6$ for wild type; $n = 6$ for *Fmr1*^{KO}; $P \leq 0.0001$) (Fig. 1 *A* and *C* and Dataset S1). Interestingly, this increase in PTEN protein levels was restored to wild-type levels when *Pten* gene dosage was reduced to half in *Fmr1*^{KO} background ($n = 6$ for wild type; $n = 4$ for *Pten*^{Het}/*Fmr1*^{KO}; $P = 0.0581$) (Fig. 1 *A* and *C* and Dataset S1). These observations indicate that PTEN protein levels are negatively regulated, possibly by FMRP based translational control. While FMRP protein levels are also increased in a *Pten*^{Het} tissue, the mechanisms through which PTEN may negatively regulate FMRP levels are likely to be indirect.

Deletion of *Pten* or *Fmr1* Genes Increase Dendritic Growth of Granule Neurons. To investigate if *Pten* and *Fmr1* genes interact to regulate dendritic growth, we examined the dentate gyrus granule neuron development in *Pten* and *Fmr1* animals. Retroviruses specifically infect dividing neurons allowing for cre-mediated deletion of floxed alleles and birth-dating of neurons (5). A mixture of Cre^{+} (pRubiC-T2A-Cre; mCherry) and Cre^{-}

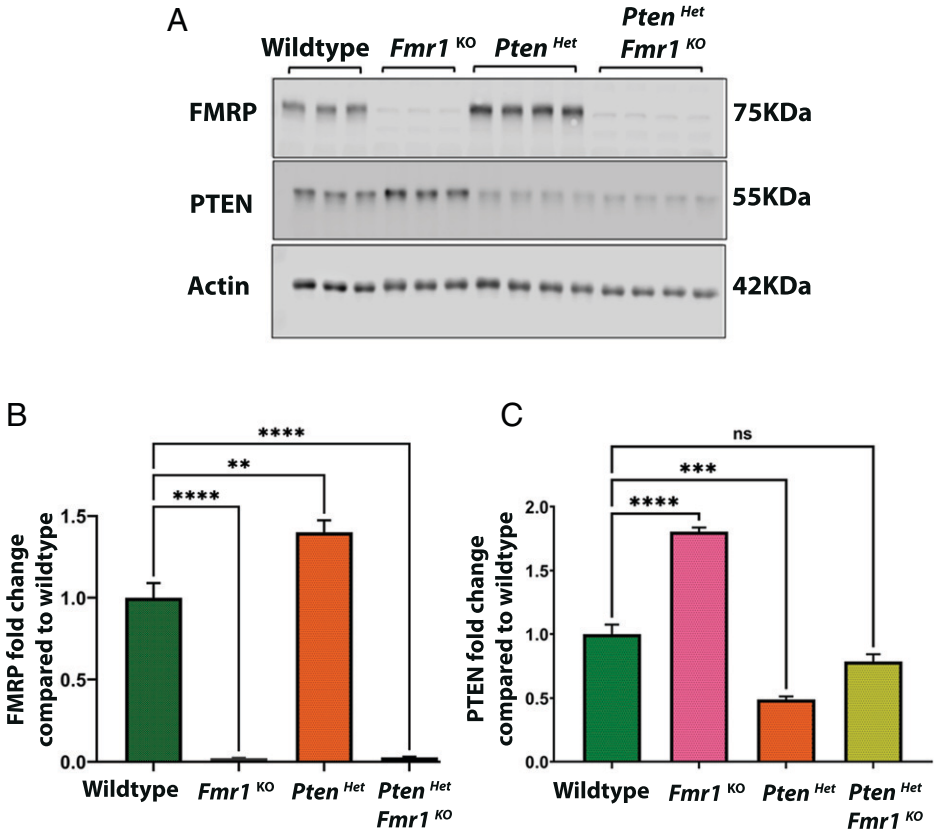

Fig. 1. PTEN protein expression is increased in *Fmr1* KO animals. (*A*) Representative Western blot images of whole hippocampal lysate from *Fmr1*^{KO}, *Pten*^{Het}, and *Pten*^{Het}/*Fmr1*^{KO} mice probed for PTEN and FMRP. (*B* and *C*) Quantitative graphs initially normalized to actin and then matched relative protein expression in the wild-type mice. $^{**}P < 0.01$, $^{***}P < 0.001$, $^{****}P < 0.0001$, and ns for nonsignificance ($P > 0.05$) calculated using one-way ANOVA with Tukey multiple comparison post hoc test.

(pRubi; green fluorescent protein [GFP]) viruses were injected into the dentate gyrus of *Pten*$^{flx/wt}$/*Fmr1*$^{flx/y}$ (*Pten* heterozygous/*Fmr1* hemizygous) and *Pten*$^{flx/flx}$/*Fmr1*$^{flx/y}$ (*Pten* homozygous/*Fmr1* hemizygous referred as *Pten*/*Fmr1* DKO) on postnatal day 7 (P7) and granule neurons cellular phenotypes were analyzed at 60 day post injection (60 DPI) (Fig. 2 *A* and *C*). With this system, wild-type cells are labeled by retrovirus expressing GFP (Cre$^-$/Control) and KO cells by retrovirus expressing mCherry (Cre$^+$) (Fig. 2 *A* and *C*). We also analyzed *Fmr1*$^{flx/y}$ (*Fmr1* hemizygous), *Pten*$^{flx/wt}$ (*Pten* heterozygous), and *Pten*$^{flx/flx}$ (*Pten* homozygous referred as *Pten* KO) (Fig. 2 *C* and *D*) using the same experimental approach.

The single-gene KOs of *Fmr1* (*Fmr1*$^{flx/y}$) and *Pten* (*Pten*$^{flx/wt}$ and *Pten*$^{flx/flx}$) showed increased granule neuron total dendritic length (Fig. 2 *C* and *D*). These observations are consistent with previously described studies (5, 14, 31–33). Compared to single (*Fmr1*$^{flx/y}$, *Pten*$^{flx/wt}$, and *Pten*$^{flx/flx}$) or double KO (*Pten*$^{flx/flx}$/*Fmr1*$^{flx/y}$) of *Pten* and *Fmr1* gene deletion, gross level morphological defects of the granule neurons are ameliorated in *Pten* heterozygous/*Fmr1* KO combination (*Pten*$^{flx/wt}$/*Fmr1*$^{flx/y}$) (Fig. 2 *C* and *D*). This suggested that *Fmr1* mutant phenotypes were being caused, at least in part, by the expression of PTEN. Therefore, we quantified the cellular phenotypes of the dentate gyrus granule neurons such as the total dendritic length, dendritic arborization, spine density, and spine length in single and combination KOs of *Pten* and *Fmr1*.

***Pten* Heterozygous, *Fmr1* Hemizygous KO Neurons Display Wild-Type Dendritic Arborization.** In 60 DPI animals, the overall dendritic length and its processes revealed an increase in *Fmr1*$^{flx/y}$ KO neurons (Cre$^-$: 1,165.41 ± 30.09, Cre$^+$: 1,301.92 ± 33.74; $P < 0.01$). *Pten*$^{flx/wt}$ KO neurons also showed a significant increase in the total dendritic length compared to their matched Cre$^-$ controls (Cre$^-$: 1,325.09 ± 34.94, Cre$^+$: 1,413.42 ± 50.30; $P < 0.0001$). *Pten* heterozygosity in *Fmr1* KO background (*Pten*$^{flx/wt}$/*Fmr1*$^{flx/y}$) led to a correction in the dendritic length, with the mean dendritic length of KO granule neurons indistinguishable from Cre$^-$ control cells (Cre$^-$: 1,394.04 ± 30.7, Cre$^+$: 1,407.20 ± 26.06; $P = 0.71$) (Fig. 2*E*; *SI Appendix*, Table 1; and Dataset S2). The observed variations in the Cre negative raw values may be due to different genetic backgrounds or animal to animal variability, thus normalizing the KO data with its respective in-tissue wild-type control neurons demonstrate the increased arborization in *Pten* heterozygotes, *Fmr1* hemizygotes and rescue of the single mutant phenotypes when the two gene deletions are combined (Fig. 2*F*).

We observed a significant increase in the total dendritic length of *Pten*$^{flx/flx}$ KO neurons (Cre$^-$: 1,230.47 ± 31.51, Cre$^+$: 1,686.12 ± 49.08; $P < 0.0001$) (Fig. 2 *G* and *H* and Dataset S2). Similar to *Pten* KO, *Pten* and *Fmr1* DKO neurons also showed a significant increase in the dendritic length (Cre$^-$: 1,343.50 ± 57.74, Cre$^+$: 1,927.29 ± 63.27; $P < 0.0001$) (Fig. 2 *G* and *H*; *SI Appendix*, Table 1; and Dataset S2). To investigate the combinational effect of heterozygous *Pten* deletion in a hemizygous *Fmr1* KO background on the dendritic arborization we performed the Sholl of length and the Sholl of intersection analyses (Fig. 3; *SI Appendix*, Fig. 6; and Datasets S3 and S7). The Sholl of length analysis between controls and KO neurons within the experimental genotypes showed 1) a significant increase in the dendritic arbor at the radial distance of 170 μm to 210 μm in *Fmr1*$^{flx/y}$ KO neurons ($P < 0.05$), suggesting a possible increase in the number of secondary and tertiary branches closer to the soma (Fig. 3*A*; *SI Appendix*, Fig. 1; and Dataset S3); 2) the *Pten*$^{flx/wt}$ mice did not display a significant increase at a specific distance from soma but do exhibit a trend of increase at every distance indicating no variation in the branching pattern (Fig. 3*B*; *SI Appendix*, Fig. 2; and Dataset S3); and 3) reduced Sholl of length in *Pten*$^{flx/wt}$/*Fmr1*$^{flx/y}$ KO neurons compared to Cre$^-$ controls at the radial distance of 190 μm and 200 μm from the soma ($P = 0.002$) suggests a decreased number of secondary and tertiary branching compared to control, which may result in reduced arborization of KO neurons (Fig. 3*C*; *SI Appendix*, Fig. 3; and Dataset S3).

Using the Sholl of intersection analysis, we examined the number of intersection points in each concentric radial junction per 10 μm outwards from the soma. The Sholl of intersection analysis performed between the Cre$^-$ and Cre$^+$ cells showed 1) a significant increase in the number of intersections at the radial junction 150 μm to 180 μm in *Fmr1*$^{flx/y}$ KO neurons indicating an increased neuronal intersection closer to the soma that leads to increased number of dendritic branching points (*SI Appendix*, Fig. 6*A* and Dataset S7) and 2) the absence of significant change at a given distance from the soma in *Pten*$^{flx/wt}$ and *Pten*$^{flx/wt}$/*Fmr1*$^{flx/y}$ KO neurons compared to their respective controls (*SI Appendix*, Fig. 6 *B* and *C* and Dataset S7). However, *Pten*$^{flx/wt}$ had more intersections overall than the control while the *Pten*$^{flx/wt}$/*Fmr1*$^{flx/y}$ displayed a trend of fewer intersections. Taken together, our data suggest that compared to single gene deletion of *Pten* or *Fmr1*, deletion of these two gene products in combination is associated with a less complex and more wild-type dendritic arbor.

Complete Loss of *Pten* and *Fmr1* Increases Dendritic Arborization. We next examined the effect of genetic deletion of both *Pten* and *Fmr1* on the granule neuron dendritic arborization and branching (Fig. 3 *D* and *E*; *SI Appendix*, Fig. 6 *D* and *E*; and Datasets S3 and S7). Differences in the Sholl of length between KO and control neurons of *Pten*$^{flx/flx}$ and *Pten*$^{flx/flx}$/*Fmr1*$^{flx/y}$ demonstrate the functional requirement of both *Pten* and *Fmr1* in the dendritic development of the granule neurons. As predicted, *Pten*$^{flx/flx}$ KO neurons showed an increase in the dendritic arbor at the radial distance from 20 μm to 60 μm ($P < 0.0001$, two-way ANOVA) and 110 μm to 190 μm ($P < 0.0001$) (Fig. 3*D*; *SI Appendix*, Figs. 4 and Dataset S7), whereas *Pten*$^{flx/flx}$/*Fmr1*$^{flx/y}$ KO neurons displayed a significant increase in Sholl length at the radial distance from 20 μm to 70 μm ($P < 0.0001$) and 100 μm to 180 μm than Cre$^-$ controls ($P < 0.0001$) (Fig. 3*E*; *SI Appendix*, Figs. 5 and Dataset S7).

KO neurons of both *Pten*$^{flx/flx}$ and *Pten*$^{flx/flx}$/*Fmr1*$^{flx/y}$ displayed an increased number of the intersections from the radial distance 10 μm to 160 μm ($P < 0.0001$, two-way ANOVA) (*SI Appendix*, Fig. 6 *D* and *E* and Dataset S7). Based on the above Sholl of length and the Sholl of intersection analysis, we suggest that both *Pten* and *Fmr1* contribute toward the growth and maturation of granule neurons dendritic morphology during the critical period of development in which activity-dependent mechanisms may play a crucial role in the overall dendritic architecture (34, 35). Our data suggest that, either complete lack of *Pten* or loss of both *Pten* and *Fmr1* gene during critical developmental time window might lead to abnormal cellular phenotypes.

***Pten* Heterozygosity Restores the Aberrant Dendritic Spines in *Fmr1* KO Neurons.** Consistent with the prior studies, compared to Cre$^-$ neurons *Fmr1*$^{flx/y}$ KO neurons showed increased spine density (Cre$^-$: 1.67 ± 0.04, Cre$^+$: 2.36 ± 0.05; $P <$

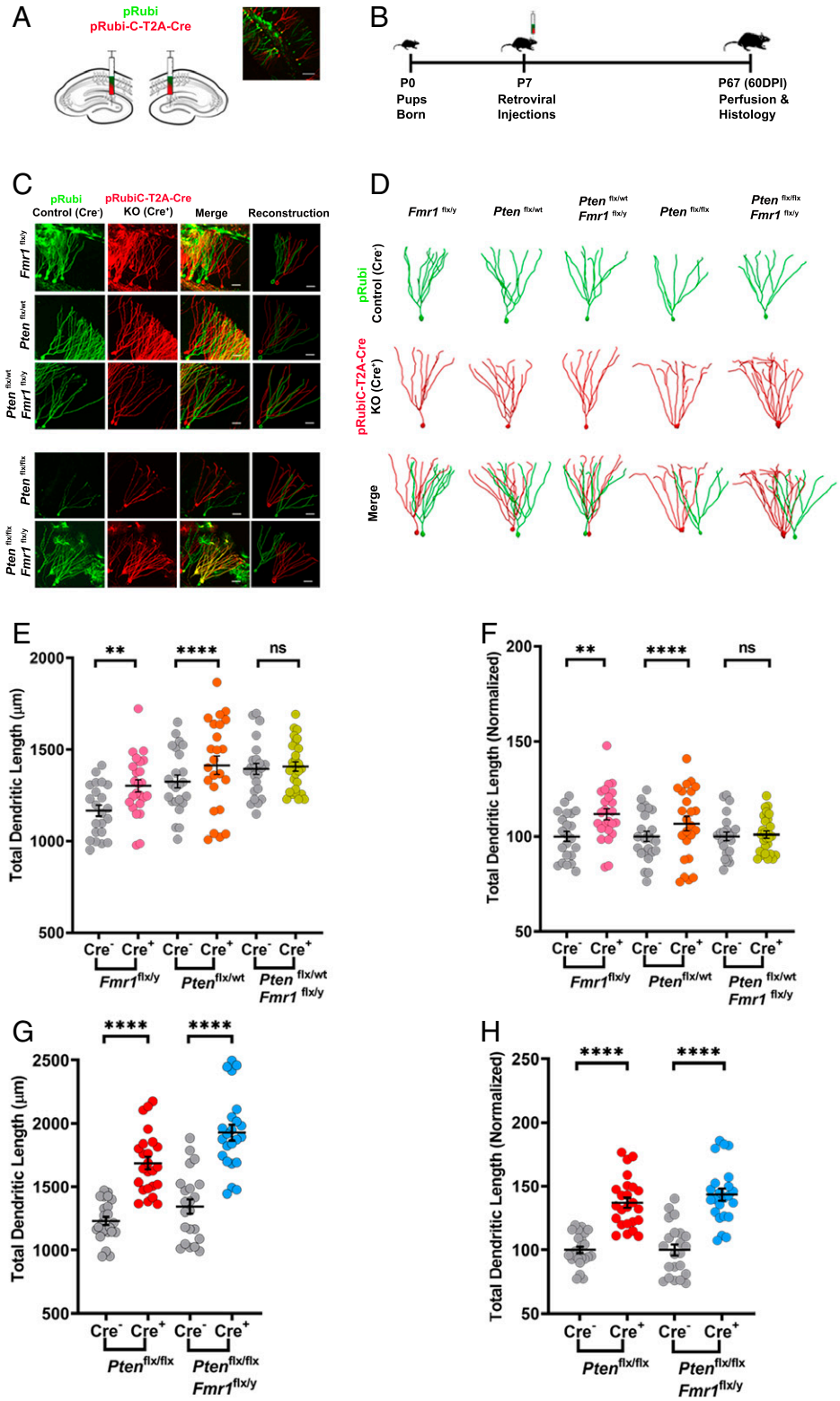

Fig. 2. Genetic deletion of *Pten* and *Fmr1* using retrovirus-mediated Cre expression alters granule neuron morphology. (*A*) Schematic shows the retroviral coinjection of pRubi and pRubiC-T2A-Cre into hippocampal dentate gyrus on P7, and the representative confocal low magnification (10×) image of dentate gyrus expressing GFP and mCherry in granule cells. (Scale bar, 70 µm.) (*B*) Schematic shows the experimental timelines: Pups were injected on P7 and all the histological analyses were performed 60 DPI (P67). (*C* and *D*) Representative (*C*) high-resolution confocal images and (*D*) three-dimensional reconstructed 60 DPI granule neurons from $Fmr1^{flx/y}$, $Pten^{flx/wt}$, $Pten^{flx/wt}/Fmr1^{flx/y}$, $Pten^{flx/flx}$, and $Pten^{flx/flx}/Fmr1^{flx/y}$ mice. (Scale bars in *C*, 50 µm.) Throughout this paper, the wild type/control (Cre^{-}) and knockout neurons (Cre^{+}) are represented in green (GFP) and red color (mCherry), respectively. (*E*) Dot plots with each dot representing an individual neuron showing the quantification of the total dendritic length in raw values and (*F*) normalized values for $Fmr1^{flx/y}$, $Pten^{flx/wt}$, and $Pten^{flx/wt}/Fmr1^{flx/y}$ and (*G* and *H*) $Pten^{flx/flx}$ (*Pten* KO) and $Pten^{flx/flx}/Fmr1^{flx/y}$ (*Pten*/*Fmr1* DKO) animals. (*E* and *F*) *Pten* heterozygous ($Pten^{flx/wt}$) and *Fmr1* KOs ($Fmr1^{flx/y}$) showed a significant increase in the total dendritic length compared to Cre^{-} controls while the $Pten^{flx/wt}/Fmr1^{flx/y}$ do not. (*G* and *H*) Both *Pten* KO and *Pten*/*Fmr1* DKO neurons showed increased dendritic length than Cre^{-} controls. Data are represented as the mean ± SEM. $^{**}P < 0.01$, $^{****}P < 0.0001$ and ns for nonsignificance ($P > 0.05$). Refer to *SI Appendix*, Table 1 for mean ± SEM, *n*, and *P* values.

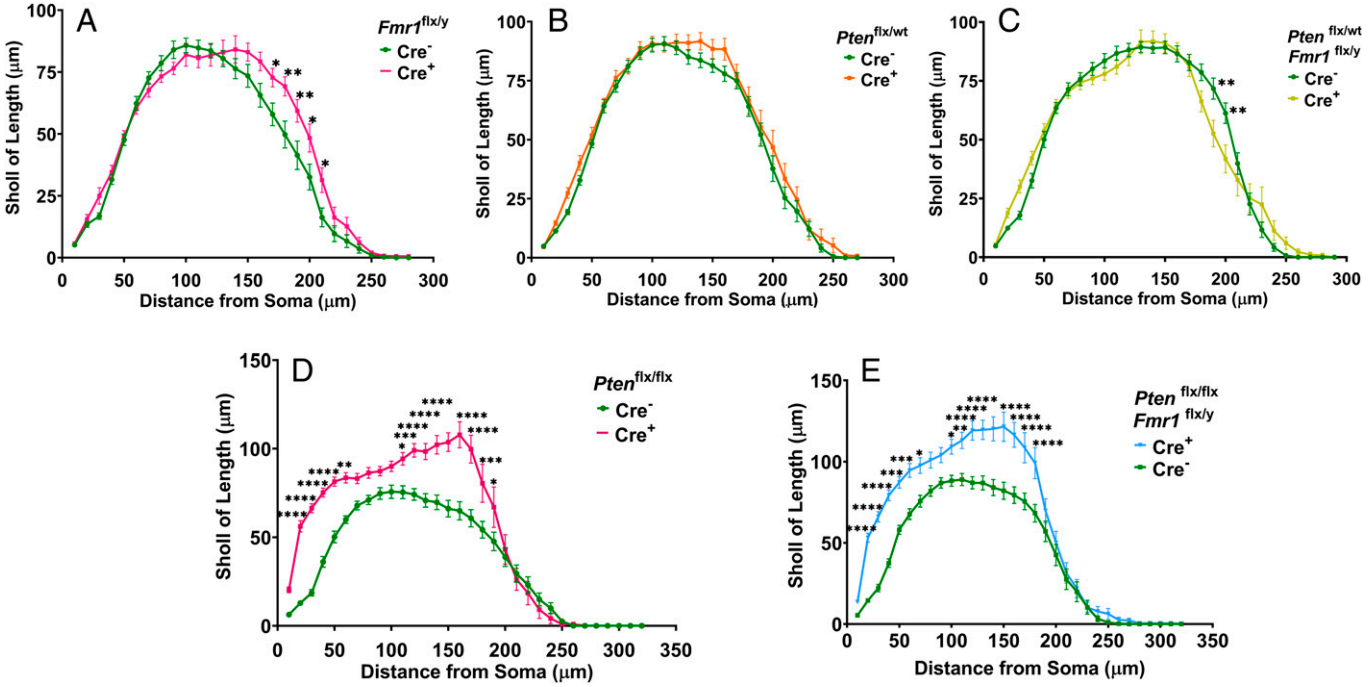

Fig. 3. *Pten* KO and *Pten*/*Fmr1* DKO increased dendritic arborization of granule neuron. Sholl of length analysis of (*A*) $Fmr1^{flx/y}$, (*B*) $Pten^{flx/wt}$, and (*C*) $Pten^{flx/wt}/Fmr1^{flx/y}$, (*D*) $Pten^{flx/flx}$, and (*E*) $Pten^{flx/flx}/Fmr1^{flx/y}$ KO neurons with their respective Cre^{-} controls. Data are represented as the mean ± SEM. $^{*}P < 0.05$, $^{**}P < 0.01$, $^{***}P < 0.001$, and $^{****}P < 0.0001$ calculated using two-way ANOVA with Bonferroni multiple comparison post hoc test.

0.0001) (Fig. 4 *A*–*C*; *SI Appendix*, Table 2; and Dataset S4) and spine length (Cre^{-}: 0.90 ± 0.01, Cre^{+}: 1.00 ± 0.05; $P < 0.004$) (Fig. 4 *F* and *G*; *SI Appendix*, Table 2; and Dataset S4). $Pten^{flx/wt}$ also showed increased spine density (Cre^{-}: 1.44 ± 0.03, Cre^{+}: 1.72 ± 0.04; $P < 0.02$) (Fig. 4 *A*–*C* and Dataset S4) while the spine length remains comparable (Cre^{-}: 0.91 ± 0.1, Cre^{+}: 0.94 ± 0.1; $P = 0.35$) (Fig. 4 *F* and *G*; *SI Appendix*, Table 2; and Dataset S4). Remarkably, the observed increase in the spine density and spine length of $Fmr1^{flx/y}$ KO neurons was corrected to Cre^{-} control levels in $Pten^{flx/wt}/Fmr1^{flx/y}$ KO neurons (Cre^{-}: 1.62 ± 0.05, Cre^{+}: 1.70 ± 0.001; $P = 0.65$) (Fig. 4 *A*–*C*; *SI Appendix*, Table 2; and Dataset S4) (Fig. 4 *F* and *G* and Dataset S4). Our data suggest that introducing *Pten* heterozygous mutation under *Fmr1* KO background can neutralize dendritic spine abnormalities associated with deficit of *Fmr1*.

Deletion of Both *Pten* and *Fmr1* Enhances the Abnormalities in Dendritic Spine Phenotypes. We next analyzed cells with both copies of *Pten* deleted. We found that complete loss of *Pten* significantly increases the dendritic spine density (Cre^{-}: 1.42 ± 0.04, Cre^{+}: 2.74 ± 0.10; $P < 0.0001$) (Fig. 4 *A*, *D*, and *E* and Dataset S4) and the spine length ($P < 0.0001$) in $Pten^{flx/flx}$ Cre^{+} neurons compared to Cre^{-} cells (Fig. 4 *H* and *I*; *SI Appendix*, Table 2; and Dataset S4). Similarly, *Pten* and *Fmr1* DKO also showed a massive increase in the spine density (Cre^{-}: 1.35 ± 0.03, Cre^{+}: 4.05 ± 0.12; $P < 0.0001$) (Fig. 4 *A*, *D*, and *E* and Dataset S4) and spine length (Fig. 4 *H* and *I*; *SI Appendix*, Table 2; and Dataset S4). The observed increase in the spine density and the spine length of $Pten^{flx/flx}/Fmr1^{flx/y}$ KO neurons is significant compared to $Pten^{flx/flx}$ KO neurons ($P < 0.0001$; Fig. 4 *D*, *E*, *H*, and *I*; *SI Appendix*, Table 2; and Dataset S4). Given the functional requirement of both *Pten* and *Fmr1* in the regulation of synaptic structure and function (36), our data suggest that inhibiting both *Pten* and *Fmr1* gene function simultaneously has a deleterious effect on the neurons resulting in abnormal dendritic spine phenotypes.

Overexpression of PTEN in $Pten^{flx/wt}/Fmr1^{flx/y}$ Cre^{+} Neurons Reduces Dendritic Length and Arborization. To investigate the effect of PTEN overexpression in $Pten^{flx/wt}/Fmr1^{flx/y}$ neurons, we delivered a mixture of retroviruses, pRubiC-T2A-Cre (mCherry, referred as Cre^{+}) and pRubi-GFP-Pten (Cre^{+} + PTEN), on P7 into the dentate gyrus, and the cellular phenotypes were studied at 60 DPI (Fig. 5*A*). In this experiment, the $Pten^{flx/wt}/Fmr1^{flx/y}$ neurons overexpressing PTEN are GFP and mCherry positive (Cre^{+} + PTEN), while all neurons expressing Cre only are labeled with mCherry (Cre^{+}) (Fig. 5 *A* and *B*). Overexpression of GFP-PTEN in $Pten^{flx/wt}/Fmr1^{flx/y}$ Cre^{+} neurons resulted in reduction in the dendritic length ($Pten^{flx/wt}/Fmr1^{flx/y}$ Cre^{+}: 1,591 ± 3.60, Cre^{+} + PTEN: 1,025 ± 3.31; $P < 0.0006$) (Fig. 5*C*; *SI Appendix*, Fig. 7; and Dataset S5). Further, the Sholl of length analysis between $Pten^{flx/wt}/Fmr1^{flx/y}$ Cre^{+} and Cre^{+} + PTEN cells revealed significant decrease in the dendritic arbor at the radial distance of 140 μm to 220 μm ($P < 0.05$) in the PTEN overexpressing neurons (Fig. 5*D*; *SI Appendix*, Fig. 7; and Dataset S5). Additionally, PTEN overexpressing neurons showed reduced Sholl of intersection values at the radius distance of 120 μm to 210 μm ($P < 0.05$) suggesting decrease in the number of secondary and tertiary branch points resulting in the overall reduction in dendritic length and arborization (Fig. 5*E*; *SI Appendix*, Fig. 7 and Dataset S5).

PTEN Overexpression Decreases the Spine Density, Spine Length, and pS6 Levels in *Fmr1* KO Neurons. We next investigated the effect of PTEN overexpression by examining phosphorylation of protein targets downstream of mTOR by analyzing pS6 (S235, 236) intensity. The brain tissue slices from $Pten^{flx/wt}/Fmr1^{flx/y}$ injected with pRubiC-T2A-Cre and pRubi-GFP-PTEN were stained for pS6 and visualized in combination with mCherry and GFP-Pten. PTEN overexpression

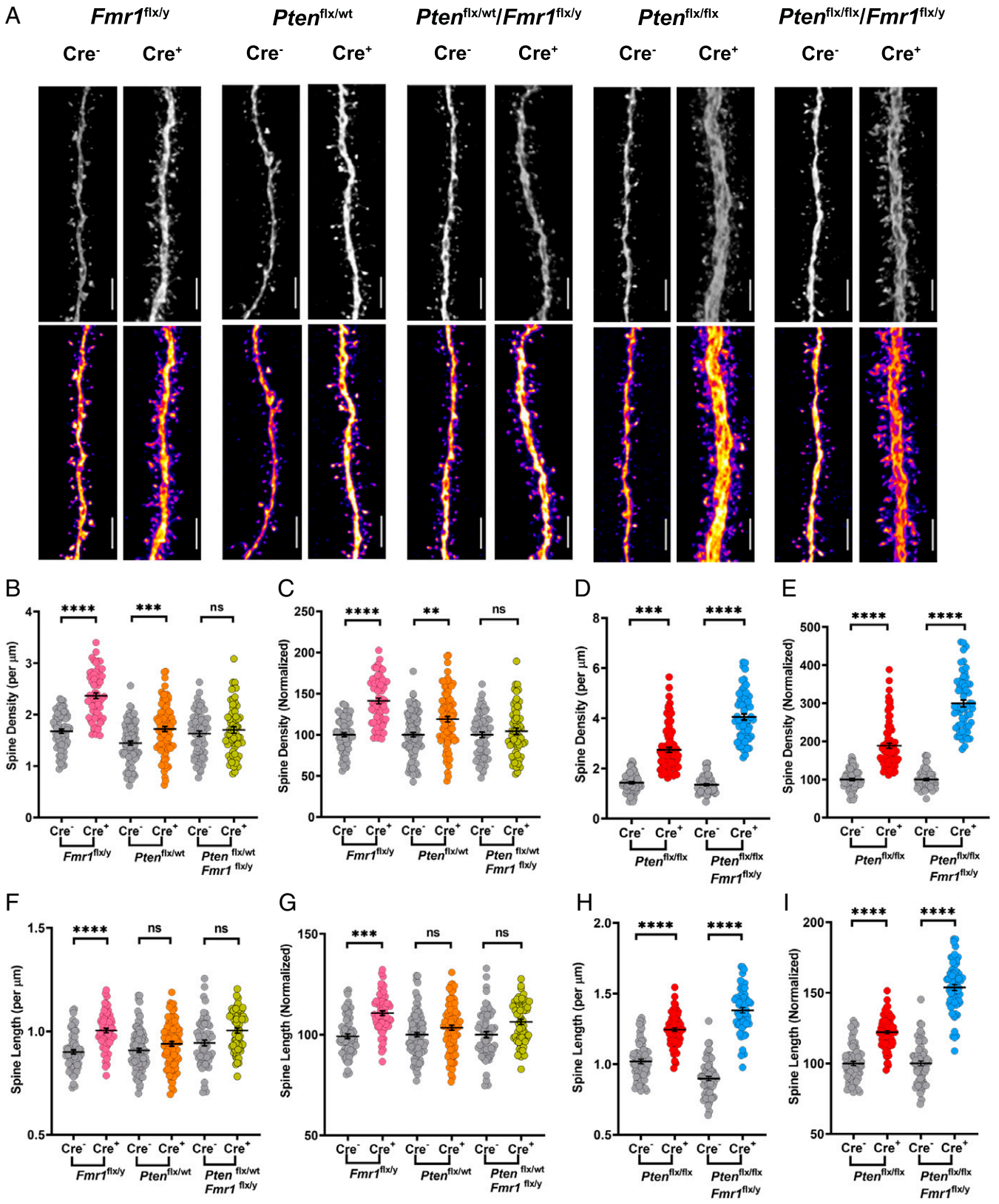

Fig. 4. *Pten* heterozygosity restores the dendritic spine density in *Fmr1* KO neurons. (*A*) Grayscale (*Top*) and pseudocolored (*Bottom*; ImageJ fire lookup table) confocal dendritic spine images of all experimental genotypes: $Fmr1^{flx/y}$, $Pten^{flx/wt}$, $Pten^{flx/wt}/Fmr1^{flx/y}$, $Pten^{flx/flx}$, and $Pten^{flx/flx}/Fmr1^{flx/y}$. (*B* and *C*) Spine density quantification (*B*) raw data and (*C*) normalized values for $Fmr1^{flx/y}$, $Pten^{flx/wt}$, and $Pten^{flx/wt}/Fmr1^{flx/y}$ granule neurons. $Pten^{flx/wt}/Fmr1^{flx/y}$ KO neurons showed reduced spine density compared to $Fmr1^{flx/y}$ KO neurons. (*D* and *E*) Quantification of the spine density for *Pten* $^{flx/flx}$ and *Pten* $^{flx/flx}/Fmr1^{flx/y}$ presented in (*D*) raw values and (*E*) normalized data. Compared to Cre^{-} controls, both *Pten* KO and *Pten*/*Fmr1* DKO neurons showed increased spine density. Data are represented in mean ± SEM. $^{**}P < 0.01$, $^{***}P < 0.001$, $^{****}P < 0.0001$, and ns for nonsignificance ($P > 0.05$). Refer to *SI Appendix*, Table 2 for mean spine density ± SEM, *P* values, number of cells, and animals. (*F*–*I*) Quantification of the spine length presented with (*F* and *G*) raw dataset and (*H* and *I*) normalized values. Dots plots in *F* and *G* correspond to $Fmr1^{flx/y}$, $Pten^{flx/wt}$, and $Pten^{flx/wt}/Fmr1^{flx/y}$ and in *H* and *I* to $Pten^{flx/flx}$ and $Pten^{flx/flx}/Fmr1^{flx/y}$ animals. (*H* and *I*) *Pten* KO and *Pten*/*Fmr1* DKO cells displayed increased spine length than Cre^{-} neurons. Data are represented in mean ± SEM. $^{***}P < 0.001$, $^{****}P < 0.0001$, and ns for nonsignificance ($P > 0.05$). Refer to *SI Appendix*, Table 2 for mean spine length ± SEM, *P* values, number of cells, and animals. (Scale bars, 3.72 µm.)

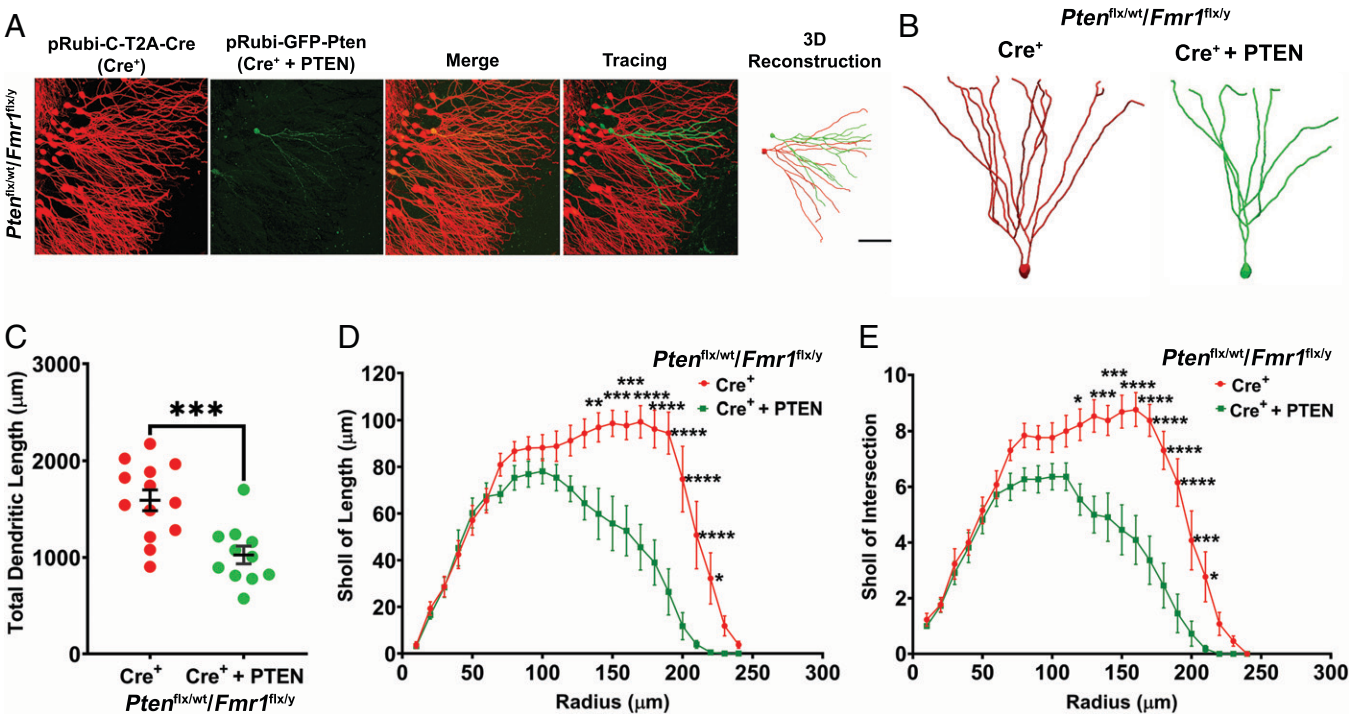

Fig. 5. PTEN overexpression in *Fmr1* KO reduce dendritic arborization and length. (*A*) The representative confocal image of granule neurons in *Pten*$^{flx/wt}$/*Fmr1*$^{flx/y}$ mice expressing pRubiC-T2A-Cre (Cre$^+$) and pRubi-GFP-PTEN (Cre$^+$ + PTEN) in hippocampal dentate gyrus. (Scale bar, 100 μm.) (*B*) A 60-DPI three-dimensional reconstruction of Cre$^+$ and Cre$^+$ + PTEN granule neurons from *Pten*$^{flx/wt}$/*Fmr1*$^{flx/y}$ animals. (*C*) Dot plots showing the quantification of total dendritic length (raw values). Each dot corresponds to an individual neuron. (*D* and *E*) Sholl of (*D*) length and (*E*) intersection between Cre$^+$ and Cre$^+$ + PTEN neurons. Data are represented in mean ± SEM. *P < 0.05, **P < 0.01, ***P < 0.001, and ****P < 0.0001 calculated using the *t* test (two-tailed) and two-way ANOVA with Bonferroni multiple comparison post hoc test.

showed reduced pS6 intensity compared to *Pten*$^{flx/wt}$/*Fmr1*$^{flx/y}$ Cre$^+$ neurons (Fig. 6 *A* and *B*, $P < 0.001$, and Dataset S6A) suggesting that PTEN overexpression in *Fmr1* KO background might be controlling the hyperactivity of mTOR signaling.

In *Fmr1* KO background we found that Cre$^+$ + PTEN neurons showed a significant decrease in spine density (*Pten*$^{flx/wt}$/*Fmr1*$^{flx/y}$ Cre$^+$: 1.37 ± 0.04, Cre$^+$ + PTEN: 1.09 ± 0.03; $P < 0.0001$) (Fig. 6 *C* and *D* and Dataset S6B) and spine length (*Pten*$^{flx/wt}$/*Fmr1*$^{flx/y}$ Cre$^+$: 1.06 ± 0.01, Cre$^+$ + PTEN: 1.01 ± 0.01; $P < 0.01$) (Fig. 6*E* and Dataset S6B) compared to *Pten*$^{flx/wt}$ Cre$^+$ neurons. Together our data suggest that PTEN overexpression in *Fmr1 KO* background, might be beneficial in terms of cellular morphology.

Discussion

Individuals with ASD or FXS display significant alteration in neuronal and synaptic structure, and such alterations are thought to be a causative factor. Genetic studies have removed key regulators in the PI3K/Akt/mTOR pathway to examine the effect on FXS pathogenesis (37). FMRP has been shown to interact directly with *Pten* mRNA via sequencing of immunoprecipitated crosslinked mRNAs (2). Here, we introduced a *Pten* heterozygous mutation in *Fmr1*$^{flx/y}$ mice and found that it restored dendritic length, neuronal arborization, excess branching, and corrected the increased spine density observed independently in *Pten* and *Fmr1* deficient mice. We found that PTEN protein levels were increased in *Fmr1* KO hippocampus and the increased PTEN levels were restored in the *Pten* heterozygous, *Fmr1* KO mice (Fig. 1). Paradoxically, complete loss of either *Pten* or *Fmr1* results in increased dendritic complexity and dendritic spines while the heterozygous reduction of *Pten* in the *Fmr1* KO results in neurons with wild-type arborization and spines. This suggests both the presence and proper balance of these two proteins is important since elimination of both does not simply cancel out opposing functions.

Protein synthesis regulation through the mTOR network is essential for synaptic organization and development in the central nervous system (38), and both FMRP and PTEN proteins are known interactors of one or more proteins in the mTOR network (1, 4–6, 33, 39–41). Mutations in a negative regulator of mTORC1 such as *Tsc1*, *Tsc2*, *Pten*, *Mnk1*, *Mnk2*, and *Fmr1* generally cause abnormal protein levels leading to a common root cause of FXS and a subset of ASDs (22, 24, 42). mTOR signaling pathway and its machinery can localize to synaptic sites where they control synaptic plasticity via regulation of local protein synthesis in dendrites and actin polymerization in spines (43, 44). In a *Pten* mouse model, the absence of PTEN leads to an increase in phosphatidylinositol (3,4,5)-triphosphate (PIP3) levels causing an excess in phosphorylated AKT and hyperactivation of the mTOR pathway (45). In the mouse model of FXS, levels of FMRP regulate mTOR signaling via PI3K upstream of the mTORC1 complex (4, 6). However, loss of FMRP also triggers hyperactivation of PI3K that causes increased protein synthesis (4). The deletion of either PTEN or FMRP exhibit hyperactivation of mTOR signaling in hippocampal neurons and overactivation of downstream mTOR targets (6, 27).

Pten deleted mice display increased levels of FMRP and phosphorylated FMRP (40). Here, we show an increased level of total PTEN protein expression in 8-wk-old *Fmr1* KO mice (Fig. 1 *A* and *C* and Dataset S1). Heterozygous *Pten* deletion in the *Fmr1* KO mouse background rectified the increased PTEN protein levels observed in *Fmr1* KO mice. In addition, we observed that FMRP levels increased in *Pten* heterozygous mice, indicating a complex reciprocal regulation. Although, FMRP may

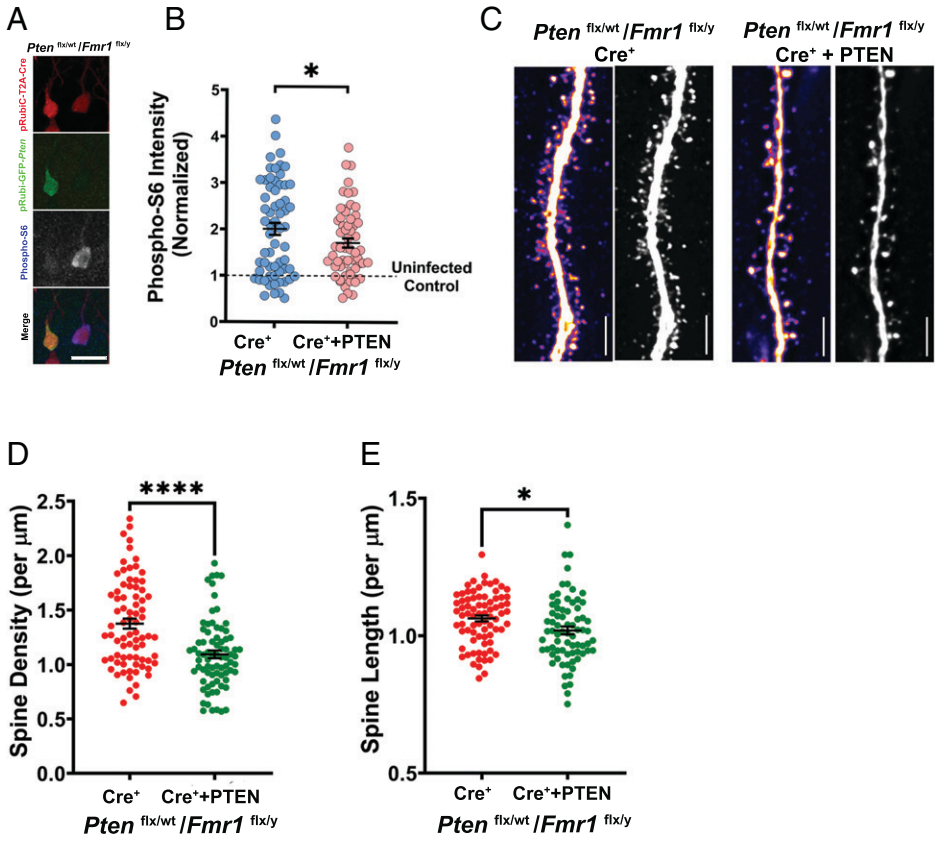

Fig. 6. Overexpression of PTEN decreases spine density, spine length, and pS6 levels in *Fmr1* KO. (*A*) Representative confocal image of Cre$^+$ (red) and Cre$^+$ + PTEN (green) cell body in *Pten*$^{flx/wt}$/*Fmr1*$^{flx/y}$ mice with pS6 staining (gray). (Scale bar, 20 µm.) (*B*) Dot plot showing the quantification of pS6 intensity. (*C*) Pseudocolored (*Left*; ImageJ fire lookup table) and grayscale (*Right*) confocal dendritic spine images of Cre$^+$ and Cre$^+$ + PTEN in *Pten*$^{flx/wt}$/*Fmr1*$^{flx/y}$. (Scale bars, 3.72 µm.) (*D* and E) Dot plots showing (*D*) spine density and (*E*) spine length quantification. Data are represented in mean ± SEM. *$P < 0.05$, and ****$P < 0.0001$ calculated using *t* test (two-tailed).

directly regulate *Pten* mRNA translation, FMRP may also indirectly regulate protein synthesis through its interaction with the mTOR network. How loss of PTEN leads to up-regulation of FMRP is less clear, but dysregulation of mTOR via PI3K and AKT may contribute to changes in FMRP levels.

FMRP localizes to both axons and synapses within the dendrites. This localization is critical for regulating neuronal morphology via FMRP transport (46, 47). Interestingly, in *Drosophila*, the *dFmr1* mutants exhibit enlarged presynaptic terminals, excessive axonal branching, and increased architectural complexity (48, 49). Twenty-eight-day-old motor neurons of *Fmr1* KO mice displayed increased amounts of dendritic arborization closer to the cell body with an increase in the number of branch points (50). We found that *Fmr1* KO neurons display increased dendritic length (Fig. 2 *E* and *F* and Dataset S2). Numerous studies conducted on *Fmr1* KO mice display excess dendritic spines with a higher proportion of immature filopodial like spines in the different brain regions (1, 31, 36, 51, 52). Variation in brain region, age, fixation protocol, and staining technique may account for the contradictions in the reported studies (53). Here, we report a substantial increase in spine density and length at 60 DPI *Fmr1*$^{flx/y}$ KO granule neurons (Fig. 4 *A*–*C* and Dataset S4).

The *Pten* gene plays a critical role in the development of dentate granule neurons of the hippocampus, thus determining the synaptic structure and function (36). Previous work from our laboratory and several others have reported that loss of *Pten* leads to ASD and alteration in neuronal morphology and physiological function (3, 8, 54, 55). Conditional *Pten* KO using different Cre-recombinase delivery methods in mice led to neuronal hypertrophy, seizures, increased dendritic arborization, and increased spine density (7, 8, 56, 57). *Pten* haploinsufficiency leads to increased dendritic arborization with ASD-related social and behavioral deficits (58). Consistent with previous studies, we found homozygous *Pten* KO neurons displayed a dramatic increase in dendritic length, neuronal arborization, and increased dendritic spine density as well as spine length (5, 14, 33, 56, 59). Our study also examined morphological features in *Pten*$^{flx/wt}$ (*Pten* heterozygous) mice showing increases in dendritic length, arbor complexity and spine density (Figs. 2 *E* and *F*, 3*B*, and 4 *A*–*C*; *SI Appendix*, Fig. 6*B*; and Datasets S2, S3, S4, and S7). While the changes are less severe than those seen in the homozygous KOs, the ability to examine Cre$^-$ control cells in the same tissue as Cre$^+$ *Pten* heterozygous cells eliminates variability resulting from animal experience and genetic background allowing us to consistently detect subtle changes.

Our data suggest that *Fmr1* and *Pten* genes interact in way that is more complex than simply opposing one another's function. It is unclear how *Pten* heterozygous deletion in the *Fmr1* hemizygote results in reduced arborization and spine density when *Pten* loss alone increases arborization and spine density. Further, exogenous overexpression of PTEN also decreases arborization and spine density in the *Pten*$^{flx/wt}$/*Fmr1*$^{flx/y}$ Cre$^+$ + PTEN cells (Figs. 5 and 6 *C*–*E* and Datasets S5 and S6 A and B). We speculate that FMRP may alter the functionality of endogenously expressed PTEN. However, when overexpressed as a cDNA any alteration in function resulting from mechanisms targeting untranslated regions of the PTEN transcript would no longer be intact. Because FMRP

has many mRNA targets, not all the cellular defects would be expected to be ameliorated by restoring PTEN levels. However, the degree of restoration we observe underscores the strength of biological impact that *Pten* loss has. Finally, it is also notable that complete loss of PTEN in *Pten*$^{flx/flx}$ cells does not further ameliorate *Fmr1* associated defects (Figs. 2 *G* and *H* and 4 *A*, *D*, *E*, *H*, and *I* and Datasets S2 and S4), consistent with the idea that proper levels of PTEN are critical for cellular development as opposed to PTEN simply antagonizing FMRP functions.

Several independent studies have demonstrated the loss of PTEN or FMRP is a likely mechanism for dysregulation of PI3K, AKT, mTOR, and p70S6K1 including cap-dependent protein translational molecules causing neurodevelopmental or neurological disease (1, 4, 6, 39–41). Our study reveals that in *Fmr1* KO mouse, genetic reduction of *Pten* gene dosage by half corrects excessive PTEN protein levels and rectifies dendritic length, complexity, and spine density. This suggests the amelioration observed in *Pten*$^{flx/wt}$/*Fmr1*$^{flx/y}$ is mediated by reduction of PTEN levels. This interpretation is strengthened by the observation that complete genetic ablation of both *Pten* and *Fmr1* displayed a greater increase in dendritic length, neuronal complexity, spine density, and length. In a *Pten*$^{flx/wt}$/*Fmr1*$^{flx/y}$ background increasing PTEN levels by overexpression further reduced multiple morphological deficits (Figs. 5 and 6), consistent with the idea that *Fmr1* mutant phenotypes are sensitive to PTEN protein levels. It will be of interest to determine the mechanistic basis through which these two ASD genes interact and of great clinical relevance to better understand how *Pten* dosage modulates phenotypes caused by loss of *Fmr1*.

Materials and Methods

Animals. Procedures involving mice were approved and performed following the Dartmouth College's Institutional Animal Care and Use Committee and the Association for the Assessment and Accreditation of Laboratory Animal Care Review Board. Conditional male KO mice (cre-lox system) used in this study are *Fmr1*$^{flx/y}$ (*Fmr1* hemizygous), *Pten*$^{flx/wt}$ (*Pten* heterozygous), *Pten*$^{flx/wt}$/*Fmr1*$^{flx/y}$ (*Pten* heterozygous and *Fmr1* hemizygous), *Pten*$^{flx/flx}$ (*Pten* homozygous), and *Pten*$^{flx/flx}$/*Fmr1*$^{flx/y}$ (*Pten/Fmr1* double homozygous). The parental lines C57BL/6J wild-type controls and B6.129S4-*Pten*^{tm1Hwu}/J homozygous (*Pten* floxed) were from the Jackson Laboratory, and *Fmr1*$^{flx/y}$ hemizygous/homozygous (*Fmr1* floxed) was a generous gift from Prof. David Nelson, Baylor College of Medicine, Houston, TX. Both *Pten* floxed and *Fmr1* floxed animals that were on a C57BL/6J genetic background were used to generate the above-mentioned experimental genotypes.

For whole-animal KO alleles, the Jackson Laboratory mice C57BL/6J, B6;129P2-*Pten*^{tm1Mak}/Mmjax (also known as m*PTEN*) and B6.129P2-*Fmr1*^{tm1Cgr}/J (*Fmr1* KO mice) were bred to generate male *Pten*^{Het}, *Fmr1*^{KO}, and *Pten*^{Het}/*Fmr1*^{KO} genotypes. All animals were housed with their littermates on a 12-h regular light/dark cycle with chow and water provided ad libitum. Data presented in this study were collected and analyzed with the experimenters blinded to genotypes.

Viral Packaging. Retrovirus containing GFP only (retrovirus with internal ubiquitin promoter; pRubi; Addgene 66696), pRubi-mCherry-T2A-Cre recombinase (pRubi-C-T2A-Cre; Addgene 66692), and pRubi-GFP-Pten were packaged and produced as previously described (60).

Stereotaxic Brain Injections. Using previously described stereotactic protocols, the retrovirus was injected into anesthetized male mice brains (61). Similarly, to test the effect of PTEN overexpression in granule neuron, we sterotaxically injected pRubi-C-T2A-Cre (mCherry) and pRubi-GFP-Pten to *Pten*$^{flx/wt}$/*Fmr1*$^{flx/y}$ (*Pten* heterozygous and *Fmr1* hemizygous) mice at P7 as previously described (61). Briefly, on P7, isoflurane-anesthetized pups were injected with 2 μL of replicative-defective retrovirus into the hippocampal dentate gyrus on both the hemisphere. From lambda, the injection coordinates are $y = \pm 1.55$, $x = \pm 1.30$, and $z = -2.3$ to -2.0. At 60 DPI, P67 animals were anesthetized using 2,2,2-tribromoethanol (Sigma Aldrich) and transcardially perfused with 4% paraformaldehyde in phosphate-buffered saline (1× PBS) containing 4% sucrose (12).

Immunohistochemistry. After perfusion, the hippocampal coronal brain slices (50 μm and 150 μm in thickness) were rinsed with 0.4% PBS containing Triton-X (0.4% PBTx) and blocked with 10% donor horse serum in PBS for 1 h at room temperature (RT). Later, the samples were incubated with primary antibodies for 48 h at 4 °C. Samples were washed with 0.4% PBTx three times, 15 min each, and labeled with fluorophore-tagged secondary antibodies for 48 h at 4 °C. Thus, immunolabeled samples were washed with 0.4% PBTx and mounted in Vectashield (H-1000, Vector Laboratories). Primary and secondary antibodies used in this study were rabbit anti-mCherry (1:5,000, Abcam, #167453), chicken anti-GFP (1:3,000, Abcam, #ab13970), rabbit anti-pS6 (1:200, Cell Signaling, #4858), anti-rabbit Cy3 peroxidase AffiniPure donkey anti-rabbit IgG (1:200, Jackson ImmunoResearch Labs, #711-035-152; RRID: AB_10015282), Alexa Fluor 488 conjugated goat anti-chicken IgY (1:200, Jackson ImmunoResearch Labs, #103-545-155; RRID: AB 2337390), and Alexa Fluor 647 conjugated goat anti-rabbit IgG (1:200, Jackson ImmunoResearch Labs, #111-605-144).

Confocal Image Analysis. Confocal images acquired using a Zeiss LSM 510 laser scanning microscope (Zeiss) were analyzed for the total dendritic arborization, the dendritic spine density, and the spine length and pS6 intensity levels as previously described (5, 14, 59). For dendritic arborization analysis, cells on the suprapyramidal blade of the dentate gyrus were imaged with a 2-μm interval and 1,024 × 1,024-pixel resolution using a 20× objective. Similarly, for the PTEN overexpressed animals, the images were acquired with a 2-μm interval and 1,024 × 1,024-pixel resolution using a 40× objective. Three-dimensional reconstruction of the whole granule neuron arbors was achieved by semiautomated tracing in Neurolucida 360 software (MBF Biosciences). For dendritic spine analysis, images were acquired with a 0.5-μm interval and 1,024 × 1,024-pixel resolution using a 63× objective and 3× optical zoom. After image deconvolution (Deconvolution Lab) (62), the quantification of dendritic spine density was performed with Neuron Studio software (14, 59, 63). For pS6 fluorescence intensity measurement, z-stacks of supra and infrapyramidal blades of dentate gyrus were acquired at 40× with a 1.3-μm oil immersion lens with 0.7× zoom, at 1,024 × 1,024 resolution with a 2-μm z-step. The Align Master plugin of ImageJ/Fiji (NIH) was utilized to account for variation in staining intensity throughout the z-stack. Further, p-S6 fluorescence intensity was normalized to the average fluorescence intensity of the control cells in the same z-stack.

Western Blot. On P67, all the experimental genotypes, *Pten*^{Het}, *Fmr1*^{KO}, and *Pten*^{Het}/*Fmr1*^{KO}, were euthanized, and the hippocampus was dissected. Samples were quickly rinsed in 1× PBS, flash frozen in liquid nitrogen, and then stored at −80 °C for further usage. Whole hippocampal lysate was prepared using a homogenization solution. After adding 600 to 700 μL of lysis buffer (1% sodium dodecyl sulfate [SDS] and 1 mM dithiothreitol in PBS), samples were homogenized with pestles and boiled at 95 °C for 5 min; samples were then cooled to RT and mixed with freshly prepared *N*-ethylmaleimide (30 mM final) (Thermo Fisher Scientific). Samples were then passed through a G25 needle two to three times, vortexed, and centrifuged for 15 min at 20,000 relative centrifugal force (RFC), and the supernatant was collected into new tubes. Just before SDS-polyacrylamide gel electrophoresis (PAGE), the protein sample was mixed 1:1 with 2× DB (250 mM Tris·HCl, pH 6.8, 2 mM ethylenediaminetetraacetic acid, 20% glycerol, 0.8% SDS, 0.02% bromophenol blue, 1,000 mM NaCl, and 4 M urea). Proteins were separated in a 10% SDS-PAGE gel and transferred to a polyvinylidene difluoride membrane (Millipore). The membrane was blocked with 1× TBS-T (20 mM Tris·HCl, pH 7.6, 136 mM NaCl, and 0.1% Tween-20) containing 3% bovine serum albumin prepared in 1× TBS-T (MP Biomedicals, LLC) for 1 h at RT. Membranes were then incubated overnight at 4 °C with the primary antibodies diluted in blocking solution. The primary antibodies used were as follows: rabbit anti-PTEN (1:1,000, Cell Signaling Technologies, #9559), rabbit anti-FMRP (1:1,000, Cell Signaling Technologies, #4317), anti-alpha actin (1:5,000, Sigma #T9026), and anti-tubulin (1:10,000, Sigma #T9026). Following the incubation in primary antibodies, membranes were washed with 1× TBS-T buffer (three times each for 5 min) and incubated with fluorescently tagged LI-COR antibodies anti-rabbit IRDye 800CW (1:15,000, #926-32211) and anti-mouse IRDye 680RD (1:15,000, #926-68070) for 1 h at 23 °C. Signals were detected by chemiluminescence or using a LI-COR fluorescent imager (64). The Western blot

images were quantified using ImageJ. Equal-sized boxes were drawn over the blots and a plot profile was generated. The area under the curve was then calculated for each band and plotted relative to the loading control.

Statistical Analysis. Sample numbers and sizes are based on similar previously published studies. To perform the statistical analysis, we used Stata 13 (StataCorp) and Prism 9 (GraphPad). For all the experimental parameters, mean ± SEM values were derived using the average values of Cre^{-} and Cre^{+} neurons. Total dendritic length, dendritic spine density, spine length, and pS6 data were analyzed as previously described (60, 65). Significance was determined by comparing cre^{+} and cre^{-} cells clustered within animals using a mixed-effect linear regression model (65). Sholl of length and Sholl of intersection analysis was performed with a two-way repeated-measure ANOVA with Bonferroni multiple comparison. One-way ANOVA with the Tukey multiple comparison test was used for quantification of the Western blot data. A two-tailed *t* test with Welch corrections was used for quantification of PTEN overexpression total dendritic length, dendritic spine density, and spine length.

Resource Availability. All retroviruses will be made available upon request, and all plasmids used in this study have been deposited with Addgene (https://www.addgene.org). Further information and requests for resources and reagents should be directed to and will be fulfilled by G.B. (giovanni.bosco@dartmouth.edu) or B.W.L. (bryan.w.luikart@dartmouth.edu).

Data Availability. Neuronal morphology data have been deposited at http://neuromorpho.org/. All of the data sets generated are included in the article and/or in the supplemental information. All retroviruses will be made available upon request, and all plasmids used in this study have been deposited with Addgene (https://www.addgene.org). Further information and requests for resources and reagents should be directed to and will be fulfilled by G.B. (giovanni.bosco@dartmouth.edu) or B.W.L. (bryan.w.luikart@dartmouth.edu).

ACKNOWLEDGMENTS. This work was funded by the Geisel School of Medicine at Dartmouth and Department of Molecular and Systems Biology (to G.B.) and the National Institutes of Mental Health (R01MH097949 to B.W.L.). We thank Meijie Li for viral packaging and Wei Wang for mouse genotyping. We would like to especially thank Stephen Barton, Patrick Skelton, and Andrew Goyette for their help. We thank Balint Kacsoh and Sassan Hodge whose *Drosophila* work originally suggested a *Pten–Fmr1* interaction. We thank all the present and previous members of Bosco and Luikart Laboratories.

1. A. Bhattacharya *et al.*, Genetic removal of p70 S6 kinase 1 corrects molecular, synaptic, and behavioral phenotypes in fragile X syndrome mice. *Neuron* **76**, 325–337 (2012).
2. J. C. Darnell *et al.*, FMRP stalls ribosomal translocation on mRNAs linked to synaptic function and autism. *Cell* **146**, 247–261 (2011).
3. P. D. Skelton, R. V. Stan, B. W. Luikart, The role of PTEN in neurodevelopment. *Mol. Neuropsychiatry* **5** (suppl. 1), 60–71 (2020).
4. C. Gross *et al.*, Excess phosphoinositide 3-kinase subunit synthesis and activity as a novel therapeutic target in fragile X syndrome. *J. Neurosci.* **30**, 10624–10638 (2010).
5. M. R. Williams, T. DeSpenza Jr., M. Li, A. T. Gulledge, B. W. Luikart, Hyperactivity of newborn Pten knock-out neurons results from increased excitatory synaptic drive. *J. Neurosci.* **35**, 943–959 (2015).
6. A. Sharma *et al.*, Dysregulation of mTOR signaling in fragile X syndrome. *J. Neurosci.* **30**, 694–702 (2010).
7. S. A. Backman *et al.*, Deletion of Pten in mouse brain causes seizures, ataxia and defects in soma size resembling Lhermitte-Duclos disease. *Nat. Genet.* **29**, 396–403 (2001).
8. C.-H. Kwon *et al.*, Pten regulates neuronal arborization and social interaction in mice. *Neuron* **50**, 377–388 (2006).
9. S. Ogawa *et al.*, A seizure-prone phenotype is associated with altered free-running rhythm in Pten mutant mice. *Brain Res.* **1168**, 112–123 (2007).
10. A. E. Clipperton-Allen, D. T. Page, Pten haploinsufficient mice show broad brain overgrowth but selective impairments in autism-relevant behavioral tests. *Hum. Mol. Genet.* **23**, 3490–3505 (2014).
11. Y. Chen, W. C. Huang, J. Séjourné, A. E. Clipperton-Allen, D. T. Page, Pten mutations alter brain growth trajectory and allocation of cell types through elevated β-Catenin signaling. *J. Neurosci.* **35**, 10252–10267 (2015).
12. B. W. Luikart *et al.*, Pten knockdown in vivo increases excitatory drive onto dentate granule cells. *J. Neurosci.* **31**, 4345–4354 (2011).
13. M. E. Haws *et al.*, PTEN knockdown alters dendritic spine/protrusion morphology, not density. *J. Comp. Neurol.* **522**, 1171–1190 (2014).
14. P. D. Skelton, P. W. Frazel, D. Lee, H. Suh, B. W. Luikart, Pten loss results in inappropriate excitatory connectivity. *Mol. Psychiatry* **24**, 1627–1640 (2019).
15. S. Braat, R. F. Kooy, The GABAA receptor as a therapeutic target for neurodevelopmental disorders. *Neuron* **86**, 1119–1130 (2015).
16. K. M. Huber, E. Klann, M. Costa-Mattioli, R. S. Zukin, Dysregulation of mammalian target of rapamycin signaling in mouse models of autism. *J. Neurosci.* **35**, 13836–13842 (2015).
17. A. Banerjee, M. F. Ifrim, A. N. Valdez, N. Raj, G. J. Bassell, Aberrant RNA translation in fragile X syndrome: From FMRP mechanisms to emerging therapeutic strategies. *Brain Res.* **1693**, 24–36 (2018).
18. C. Bagni, F. Tassone, G. Neri, R. Hagerman, Fragile X syndrome: Causes, diagnosis, mechanisms, and therapeutics. *J. Clin. Invest.* **122**, 4314–4322 (2012).
19. D. L. Nelson, H. T. Orr, S. T. Warren, The unstable repeats–Three evolving faces of neurological disease. *Neuron* **77**, 825–843 (2013).
20. E. M. Berry-Kravis *et al.*, Drug development for neurodevelopmental disorders: Lessons learned from fragile X syndrome. *Nat. Rev. Drug Discov.* **17**, 280–299 (2018).
21. V. Martínez-Cerdeño, Dendrite and spine modifications in autism and related neurodevelopmental disorders in patients and animal models. *Dev. Neurobiol.* **77**, 393–404 (2017).
22. B. S. Abrahams, D. H. Geschwind, Advances in autism genetics: On the threshold of a new neurobiology. *Nat. Rev. Genet.* **9**, 341–355 (2008).
23. H. Y. Zoghbi, M. F. Bear, Synaptic dysfunction in neurodevelopmental disorders associated with autism and intellectual disabilities. *Cold Spring Harb. Perspect. Biol.* **4**, a009886 (2012).
24. M. Subramanian, C. K. Timmerman, J. L. Schwartz, D. L. Pham, M. K. Meffert, Characterizing autism spectrum disorders by key biochemical pathways. *Front. Neurosci.* **9**, 313 (2015).
25. S. C. Borrie, H. Brems, E. Legius, C. Bagni, Cognitive dysfunctions in intellectual disabilities: The contributions of the Ras-MAPK and PI3K-AKT-mTOR pathways. *Annu. Rev. Genomics Hum. Genet.* **18**, 115–142 (2017).
26. J. C. Darnell, E. Klann, The translation of translational control by FMRP: Therapeutic targets for FXS. *Nat. Neurosci.* **16**, 1530–1536 (2013).
27. J. A. Ronesi *et al.*, Disrupted Homer scaffolds mediate abnormal mGluR5 function in a mouse model of fragile X syndrome. *Nat. Neurosci.* **15**, 431–440, S1 (2012).
28. A. Bhattacharya *et al.*, Targeting translation control with p70 S6 kinase 1 inhibitors to reverse phenotypes in fragile X syndrome mice. *Neuropsychopharmacology* **41**, 1991–2000 (2016).
29. B. D. Auerbach, E. K. Osterweil, M. F. Bear, Mutations causing syndromic autism define an axis of synaptic pathophysiology. *Nature* **480**, 63–68 (2011).
30. T. Maurin, S. Zongaro, B. Bardoni, Fragile X syndrome: From molecular pathology to therapy. *Neurosci. Biobehav. Rev.* **46**, 242–255 (2014).
31. A. W. Grossman, G. M. Aldridge, I. J. Weiler, W. T. Greenough, Local protein synthesis and spine morphogenesis: Fragile X syndrome and beyond. *J. Neurosci.* **26**, 7151–7155 (2006).
32. A. W. Grossman *et al.*, Developmental characteristics of dendritic spines in the dentate gyrus of Fmr1 knockout mice. *Brain Res.* **1355**, 221–227 (2010).
33. S. A. Getz, T. DeSpenza Jr., M. Li, B. W. Luikart, Rapamycin prevents, but does not reverse, aberrant migration in Pten knockout neurons. *Neurobiol. Dis.* **93**, 12–20 (2016).
34. R. G. Kalb, Regulation of motor neuron dendrite growth by NMDA receptor activation. *Development* **120**, 3063–3071 (1994).
35. F. M. Inglis, K. E. Zuckerman, R. G. Kalb, Experience-dependent development of spinal motor neurons. *Neuron* **26**, 299–305 (2000).
36. H. Ito, R. Morishita, K. I. Nagata, Autism spectrum disorder-associated genes and the development of dentate granule cells. *Med. Mol. Morphol.* **50**, 123–129 (2017).
37. C. Gross *et al.*, Increased expression of the PI3K enhancer PIKE mediates deficits in synaptic plasticity and behavior in fragile X syndrome. *Cell Rep.* **11**, 727–736 (2015).
38. D. R. Hampson, S. Gholizadeh, L. K. K. Pacey, Pathways to drug development for autism spectrum disorders. *Clin. Pharmacol. Ther.* **91**, 189–200 (2012).
39. J. N. Lugo, G. D. Smith, J. B. Morrison, J. White, Deletion of PTEN produces deficits in conditioned fear and increases fragile X mental retardation protein. *Learn. Mem.* **20**, 670–673 (2013).
40. J. N. Lugo *et al.*, Deletion of PTEN produces autism-like behavioral deficits and alterations in synaptic proteins. *Front. Mol. Neurosci.* **7**, 27 (2014).
41. A. R. White, D. Tiwari, M. C. MacLeod, S. C. Danzer, C. Gross, PI3K isoform-selective inhibition in neuron-specific PTEN-deficient mice rescues molecular defects and reduces epilepsy-associated phenotypes. *Neurobiol. Dis.* **144**, 105026 (2020).
42. J. Zhou, L. F. Parada, PTEN signaling in autism spectrum disorders. *Curr. Opin. Neurobiol.* **22**, 873–879 (2012).
43. W. Huang *et al.*, mTORC2 controls actin polymerization required for consolidation of long-term memory. *Nat. Neurosci.* **16**, 441–448 (2013).
44. S. J. Tang *et al.*, A rapamycin-sensitive signaling pathway contributes to long-term synaptic plasticity in the hippocampus. *Proc. Natl. Acad. Sci. U.S.A.* **99**, 467–472 (2002).
45. A. Di Cristofano, P. P. Pandolfi, The multiple roles of PTEN in tumor suppression. *Cell* **100**, 387–390 (2000).
46. L. N. Antar, J. B. Dictenberg, M. Plociniak, R. Afroz, G. J. Bassell, Localization of FMRP-associated mRNA granules and requirement of microtubules for activity-dependent trafficking in hippocampal neurons. *Genes Brain Behav.* **4**, 350–359 (2005).
47. L. N. Antar, R. Afroz, J. B. Dictenberg, R. C. Carroll, G. J. Bassell, Metabotropic glutamate receptor activation regulates fragile x mental retardation protein and FMR1 mRNA localization differentially in dendrites and at synapses. *J. Neurosci.* **24**, 2648–2655 (2004).
48. H. L. Zhang *et al.*, Neurotrophin-induced transport of a β-actin mRNP complex increases β-actin levels and stimulates growth cone motility. *Neuron* **31**, 261–275 (2001).
49. L. Pan, Y. Q. Zhang, E. Woodruff, K. Broadie, The *Drosophila* fragile X gene negatively regulates neuronal elaboration and synaptic differentiation. *Curr. Biol.* **14**, 1863–1870 (2004).
50. C. C. Thomas, C. L. Combe, K. A. Dyar, F. M. Inglis, Modest alterations in patterns of motor neuron dendrite morphology in the Fmr1 knockout mouse model for fragile X. *Int. J. Dev. Neurosci.* **26**, 805–811 (2008).
51. T. V. Bilousova *et al.*, Minocycline promotes dendritic spine maturation and improves behavioural performance in the fragile X mouse model. *J. Med. Genet.* **46**, 94–102 (2009).
52. J. Levenga *et al.*, Subregion-specific dendritic spine abnormalities in the hippocampus of Fmr1 KO mice. *Neurobiol. Learn. Mem.* **95**, 467–472 (2011).
53. C. X. He, C. Portera-Cailliau, The trouble with spines in fragile X syndrome: Density, maturity and plasticity. *Neuroscience* **251**, 120–128 (2013).
54. T. W. Frazier *et al.*, Molecular and phenotypic abnormalities in individuals with germline heterozygous PTEN mutations and autism. *Mol. Psychiatry* **20**, 1132–1138 (2015).
55. T. W. Frazier *et al.*; Developmental Synaptopathies Consortium, Cross-level analysis of molecular and neurobehavioral function in a prospective series of patients with germline heterozygous PTEN mutations with and without autism. *Mol. Autism* **12**, 5 (2021).

56. R. Y. K. Pun *et al.*, Excessive activation of mTOR in postnatally generated granule cells is sufficient to cause epilepsy. *Neuron* **75**, 1022–1034 (2012).
57. C.-H. Kwon *et al.*, Pten regulates neuronal soma size: A mouse model of Lhermitte-Duclos disease. *Nat. Genet.* **29**, 404–411 (2001).
58. W. C. Huang, Y. Chen, D. T. Page, Hyperconnectivity of prefrontal cortex to amygdala projections in a mouse model of macrocephaly/autism syndrome. *Nat. Commun.* **7**, 13421 (2016).
59. P. D. Skelton, J. Poquerusse, J. R. Salinaro, M. Li, B. W. Luikart, Activity-dependent dendritic elaboration requires Pten. *Neurobiol. Dis.* **134**, 104703 (2020).
60. C. J. Fricano-Kugler, M. R. Williams, J. R. Salinaro, M. Li, B. Luikart, Designing, packaging, and delivery of high titer CRISPR retro and lentiviruses via stereotaxic injection. *J. Vis. Exp.* **111**, 53783 (2016).
61. B. W. Luikart *et al.*, miR-132 mediates the integration of newborn neurons into the adult dentate gyrus. *PLoS One* **6**, e19077 (2011).
62. D. Sage *et al.*, DeconvolutionLab2: An open-source software for deconvolution microscopy. *Methods* **115**, 28–41 (2017).
63. A. Rodriguez, D. B. Ehlenberger, D. L. Dickstein, P. R. Hof, S. L. Wearne, Automated three-dimensional detection and shape classification of dendritic spines from fluorescence microscopy images. *PLoS One* **3**, e1997 (2008).
64. R. Chakrabarti *et al.*, INF2-mediated actin polymerization at the ER stimulates mitochondrial calcium uptake, inner membrane constriction, and division. *J. Cell Biol.* **217**, 251–268 (2018).
65. E. L. Moen, C. J. Fricano-Kugler, B. W. Luikart, A. J. O'Malley, Analyzing clustered data: Why and how to account for multiple observations nested within a study participant? *PLoS One* **11**, e0146721 (2016).